Published in final edited form as:
Clin Cancer Res. 2010 October 15; 16(20): 4968–4977. doi:10.1158/1078-0432.CCR-10-0969.

Radiation-guided drug delivery to mouse models of lung cancer

Ghazal Hariri[1], **Heping Yan**[2], **Hailun Wang**[1], **Zhaozhong Han**[1], and **Dennis E. Hallahan**[1,2,3]

[1]Department of Radiation Oncology, Vanderbilt University,1301 Medical Center Drive, B902 TVC, Nashville, Tennessee, 37232, USA

[2]Department of Radiation Oncology, Mallinckrodt Institute of Radiology, Washington University School of Medicine, St. Louis, Missouri, 63110, USA

[3]Siteman Cancer Center, Washington University School of Medicine, St. Louis, Missouri, 63110, USA

Abstract

Purpose—The purpose of this study was to achieve improved cancer-specific delivery and bioavailability of radiation-sensitizing chemotherapy using radiation-guided drug delivery.

Experimental Design—Phage display technology was used to isolate a recombinant peptide (HVGGSSV) that binds to a radiation-inducible receptor in irradiated tumors. This peptide was used to target nab-paclitaxel to irradiated tumors, achieving tumor-specificity and enhanced bioavailability of paclitaxel.

Results—Optical imaging studies showed that HVGGSSV guided nab-paclitaxel selectively targeted irradiated tumors and showed 1.48 ± 1.66 photons/s/cm^2/sr greater radiance compared to SGVSGHV-nab-paclitaxel, and 1.49 ± 1.36 photons/s/cm^2/sr greater than nab-paclitaxel alone ($p<0.05$). Biodistribution studies showed more than 5-fold increase in paclitaxel levels within irradiated tumors in HVGGSSV-nab-paclitaxel treated groups as compared to either nab-paclitaxel or SGVSGHV-nab-paclitaxel at 72 hrs. Both LLC and H460 lung carcinoma murine models showed significant tumor growth delay for HVGGSSV-nab-paclitaxel as compared to nab-paclitaxel, SGVSGHV-nab-paclitaxel and saline controls. HVGGSSV-nab-paclitaxel treatment induced a significantly greater loss in vasculature in irradiated tumors compared to unirradiated tumors, nab-paclitaxel, SGVSGHV-nab-paclitaxel, and untreated controls.

Conclusions—HVGGSSV nab-paclitaxel was found to bind specifically to the TIP-1 receptor expressed in irradiated tumors, enhance bioavailability of paclitaxel, and significantly increase tumor growth delay as compared to controls in mouse models of lung cancer. Here we show that targeting nab-paclitaxel to radiation-inducible TIP-1 results in increased tumor-specific drug delivery and enhanced biological efficacy in the treatment of cancer.

Keywords

nanoparticles; cancer; targeting; radiation; drug delivery

Statement of Translational Relevance

Ionizing radiation can be used to induce the expression of cell surface molecules unique to cancer. Phage displayed peptide libraries can be used to discover peptides that bind

*Correspondence: Dennis E. Hallahan, M.D., Elizabeth H. and James S. McDonnell III, Distinguished Professor and Department Head, Washington University School of Medicine, Department of Radiation Oncology, Address: 4511 Forest Park Ave., Suite 200, St. Louis, MO 63108, dhallahan@WUSTL.edu, Phone: (314) 362 9700, Fax: (314) 747 5498.

specifically to irradiated cancers. Here, we show that the amino acid sequence HVGGSSV achieved tumor-specific binding when conjugated to nanoparticles containing radiation-sensitizing paclitaxel. Radiation-guided delivery of nanoparticles improved both bioavailability of drug delivery and efficacy of radiotherapy in mouse models of lung cancer. Further studies are necessary to determine whether improved cancer-specific delivery of radiation-sensitizing chemotherapy translates to reduced side effects and better treatment outcomes in lung cancer patients.

Introduction

Drug delivery systems have been developed to increase drug delivery to cancer and thereby enhance therapeutic response (1-3). Examples of drug delivery systems include liposomal doxorubicin and nanoparticle albumin-bound paclitaxel (nab-paclitaxel) (4), which are not ligand-targeted systems and therefore not *tumor-specific* (5-7). Nab-paclitaxel has features that make it an appropriate vehicle for drug encapsulation (8-10). It is a natural carrier of hydrophobic molecules such as paclitaxel, and has non-covalent binding characteristics (11). This allows paclitaxel to bind reversibly to albumin. Nab-paclitaxel binds to the albumin receptor, gp60, which is ubiquitously present throughout tissues (12-14), and therefore does not reduce the incidence of complications (15-17).

Physical energy has been used to achieve site-specific drug delivery to cancer. For example, heat is used to release drugs from liposomes and nanocages. These technologies are complemented by use of radiation-guided peptides conjugated to nab-paclitaxel. Ligands that can specifically target receptors within tumor microvasculature have been previously investigated (18,3). Radiation can be used to achieve site-specific expression of receptors within cancer (19,20). These radiation-inducible receptors can in turn be targeted by peptides selected through phage display technology (22). Nanoparticle carriers can be functionalized with these peptide ligands to enable radiation-guided delivery of chemotherapeutic drugs to tumor microvasculature (19-24). This tumor-specific delivery of chemotherapy has the potential to improve treatment tolerability by reducing non-specific delivery of cytotoxic drugs to normal tissues and improve bioavailability of chemotherapy to cancer.

We studied nab-paclitaxel as a scaffold for creating a radiation-guided drug delivery system. To increase tumor-specific delivery of paclitaxel and enhance tumor bioavailability, we functionalized nab-paclitaxel with a radiation-guided peptide (HVGGSSV) that specifically targets microvasculature within irradiated tumors. In this study, we focused on non-small cell lung cancer because concomitant chemotherapy and radiation therapy improves survival (30-34). By using radiation-guided peptides conjugated to nab-paclitaxel, we retargeted nab-paclitaxel from the non-specific albumin receptor gp60 to a radiation-inducible receptor. This approach improved tumor-specific delivery of nab-paclitaxel, enhanced bioavailability within tumors, and enhanced therapeutic efficacy in the treatment of mouse models of lung cancer.

Materials and Methods

Cell culture and reagents

The tumor cell lines used were murine Lewis Lung Carcinoma (LLC) and NCI-H460 human large cell lung carcinoma, obtained from American Type Culture Collection (ATCC; Rockville, MD). Nab-paclitaxel was supplied by American Bioscience, Inc. (Santa Monica, CA). The compound was dissolved in 0.9% NaCl solution to a concentration of 5 mg/mL

and administered i.v. in a concentration of 10 mg/kg (paclitaxel). In all experiments, nab-paclitaxel was given once as a single tail vein injection without premedication.

Conjugation chemistry

Nab-paclitaxel (purchased from Abraxis, Bridgewater, NJ) was conjugated to a heterobifunctional cross-linker, succinimidyl-[(*N*-maleimidopropionamido)-tetraethyleneglycol] ester (Pierce Biotechnology, Rockford, IL), producing a maleimide functionalized nab-paclitaxel surface. The cysteine thiol group of CGGGKKKGGGNHVGGSSV (21) was reacted with the maleimide functionalized surface to produce HVGGSSV labeled nab-paclitaxel. A scrambled version of HVGGSSV peptide (CGGGKKKGGGSGVSGHVN) was used as a control and conjugated to nab-paclitaxel in the same manner. For *in vivo* near-infrared (NIR) imaging, the above conjugates were labeled with near-infrared fluorescent probe Alexa fluor 750. Monofunctional N-hydroxysuccinamide (NHS) esters of Alexa fluor 750 were conjugated to the lysine ε-amino groups on the peptide for near-infrared fluorescence imaging. For conjugation, 1 mg Alexa fluor 750 was dissolved in 100 ul of dimethyl sulfoxide (Sigma, St. Louis, MO) and added to HVGGSSV modified nab-paclitaxel for 1 hr in a phosphate buffered saline buffer at a pH of 7.

Animal Models

Animal studies were performed according to a protocol approved by Vanderbilt's IACUC. Male athymic nude mice (nu/nu) between four to six weeks old (Harlan Inc., Indianapolis IN, USA) or C57BL6 male mice were anesthetized using a ketamine and xylazine solution before being injected subcutaneously in the hind legs with 1×10^6 LLC or H460 cells suspended in 100 μL sterile phosphate buffered saline. One week after inoculation, the tumors reached an approximate size of 0.5-0.8 cm in diameter, and the mice were used for studies.

Radiation and treatment protocol

Tumors were allowed to reach 0.5-0.8 cm^3 in size before beginning treatments. All mice were anesthetized using ketamine and xylazine solution prior to irradiation to inhibit mobility during treatment. Tumors were irradiated with 300kV X-rays using a Pantak Therapax 3 linear accelerator system (Pantak, East Haven, CT) with an adjustable collimator set to limit dosage to the tumor region only. During irradiation procedures, 1 cm thick lead blocks were arranged above the rest of the body, leaving only the desired area on the hind limb exposed for treatment. Four hours following radiation, mice were administered drug treatments through tail vein injection.

Imaging and image analysis

In vivo NIR imaging was performed with a Xenogen IVIS 200 small animal imaging system (Xenogen Inc., Alameda CA, USA) with a Cy7 filter set (excitation at 680 nm and emission at 775 nm). Nude mice bearing LLC or H460 lung carcinoma tumors implanted in both hind limbs were treated with radiation. The tumor on the left side of each mouse received a radiation dose of 3 Gy and the tumor on the right side received no radiation (sham radiation dose of 0 Gy) and served as an internal negative control. Four hours following irradiation, mice were anesthetized using an intraperitoneal injection of ketamine and xylazine and prepared for tail vein injections of the treatment conjugates. At 72 hrs post-injection, all mice were anesthetized with isoflurane and imaged with the Xenogen IVIS. All NIR images were acquired with one second exposure time using an f/stop of 2. For quantitative comparison, regions of interest (ROIs) were drawn over tumors, and the total radiance (p/s/cm^2/sr) for each area was measured. Results are presented as mean and SEM for a group of

3-6 animals. Values for treated groups were compared to controls with the unpaired Student's t test.

Biodistribution analysis

6-8 week old male C57BL6 mice with subcutaneous LLC murine lung carcinoma tumors were injected i.v. with 10 mg/kg (paclitaxel) nab-paclitaxel, targeted HVGGSSV-nab-paclitaxel or SGVSGHV-nab-paclitaxel. Mice were sacrificed at 12 and 72 hrs after administration, vital organs were excised and blood samples collected by cardiac puncture. Tissues were immediately homogenized and kept on ice. Each sample was spiked with an internal standard of docetaxel, followed by solid-phase extraction with acetonitrile, and centrifuged at 3000 rpm (25). Supernatant was removed and analyzed for paclitaxel content using HPLC- MS/MS. Results are presented as mean and SEM for a group of 3 animals.

Subcutaneous tumor models

6-8 week old male athymic nude mice or C57BL6 mice were injected heterotopically with either 1×10^6 H460 human lung carcinoma cells or 10^6 murine Lewis lung carcinoma cells, respectively. Mice were monitored daily and tumor volume was measured manually with a caliper, using the formula volume = length × width × height/2 derived from the formula for an ellipsoid. When tumors had reached the desired size (5-6 mm diameter), the mice were grouped (n = 5) and injected intravenously with PBS, nab-paclitaxel, targeted HVGGSSV-nab-paclitaxel or SGVSGHV-nab-paclitaxel at a dose of 10 mg/kg of paclitaxel. All mice were grouped as follows: saline only, radiation only (3Gy × 3), nab-paclitaxel (3 Gy), nab-paclitaxel with radiation (3Gy × 3), targeted HVGGSSV-nab-paclitaxel (3 Gy), targeted HVGGSSV-nab-paclitaxel with radiation (3Gy × 3), SGVSGHV-nab-paclitaxel (3 Gy), SGVSGHV-nab-paclitaxel with radiation (3Gy × 3). Radiation treatment was administered every other day (28). Data were calculated as fold increase from the original tumor volume, with variance analyzed by the Kruskal-Wallis method (35).

Anti Tip 1 monoclonal antibody production and purification

Mouse—Tip1 protein was produced in bacteria and purified using GST columns. BALB/C mice were initially immunized with 50 mg of Tip-1 antigen mixed with equivalent amounts of Titermax adjuvant (CytRx Corporation) for each mouse. One month after initial immunization, mice were boosted with equivalent amounts of antigen without adjuvant two to three times at two week intervals. The mouse anti-Tip-1 polyclonal antibody titer was evaluated by ELISA and Western blot methods. Mice exhibiting high immune response to Tip-1 antigen were chosen as B cell donors. Spleen were removed and homogenized in RPMI 1640 culture medium free of serum and other additives. Spleen cells were combined with Sp2/O mouse meyloma (2×10^7 per spleen). Mixed cells were washed twice and centrifuged at 1200 rpm for 8 minutes at room temperature. Supernatant was removed, and the cell pellet was lightly agitated to loosen the cells. Approximately 1 ml PEG (polyethylene glycol 1500) (Roche) was added to fuse the cells. The fused cells were washed once with plain medium and finally re-suspended in RPMI 1640 medium supplemented with 10% fetal bovine serum (Gemini Bioproducts, CA), L-glutamine, antibiotics and HAT (Sigma), plated into 24 well tissue culture plates and incubated at 37° C in a humidified CO_2 incubator. Fifteen days after fusion, hybridoma culture supernatants were removed from individual wells and transferred to separate 96 well microtiter plates for ELISA, Western blot and antibody printing assays against Tip-1 antigen. Hybridomas that produced antibodies positive by immunoassay were chosen for sub-cloning by using limiting dilution. Resulting single-cell clones were retested by the aforementioned methods to detect antigen-positive monoclonal antibody-producing hybridomas. Positive hybridoma clones were transferred to individual flasks to expand cell number from one cell clone, and

incubated with serum-free medium for antibody production. The antibodies produced by positive clones in serum-free medium were harvested twice a week for further monoclonal antibody purification. Filtered monoclonal antibody collected from serum-free medium was purified by protein A and protein G columns. The concentrated purified monoclonal antibody was assayed and stored at -20° C.

Rabbit and Guinea Pig—Tip-1 protein was synthesized in bacteria as above. Rabbits (New Zealand white) or Guinea pigs were initially immunized with 100 mg of Tip-1 antigen mixed with equivalent amounts of Titermax adjuvant (CytRx Corporation). One month after initial immunization, the animals were boosted with equivalent amounts of antigen two or three times at 2 week intervals without adjuvant. The animals were sacrificed and blood was collected. Serum was separated individually when antibody titer reached desired titer, and evaluated by ELISA and Western blot assays. Rabbit whole IgG in serum was purified through protein A and protein G columns and guinea pig total IgG in serum was harvested through Protein A columns. Anti-Tip-1 IgG was purified and sequentially passed on TIP-1 conjugated to cyanogens activated in sepharose 4B beads (Sigma). The antibody was dialyzed against PBS and then concentrated. Antibody concentration was tested by the Bradford protein assay method. The purified anti-Tip-1 IgG was stored at -20° C.

Immunohistochemistry

LLC murine lung tumors were implanted into the hind limbs of C57BL6 mice and grown to a diameter of approximately 8-10 mm. Tumors were irradiated with 0 Gy or 3 Gy, and administered either drug or antibody treatments approximately 5 hrs after irradiation. For TIP-1 staining, formaldehyde fixed paraffin embedded sections were treated with TIP-1 primary antibody and anti-rabbit secondary antibody (Sigma), and counterstained with hematoxylin.

For colocalization study, mice were treated with Alexa fluor 594 labeled HVGGSSV-nab-paclitaxel, SGVSGHV-nab-paclitaxel, nab-paclitaxel, or no treatment. Mice were sacrificed and tumors excised at 3 hrs. Tissues were frozen in OCT embedding medium followed by liquid nitrogen. Cryosections of 5 μm thickness were immunostained using FITC labeled rabbit anti-von Willebrand factor antibody (Dako). Images were captured on a Zeiss Axiophot widefield microscope using oil immersion at 60x.

For paclitaxel staining, mice were treated with HVGGSSV-nab-paclitaxel, SGVSGHV-nabpaclitaxel, nab-paclitaxel, or no treatment. Mice were sacrificed and tumors excised approximately 12-16 hrs. For detection of drug presence in tissues, a mouse anti-paclitaxel monoclonal antibody (Santa Cruz) was used (29).

For apoptosis detection, mice were treated with HVGGSSV-nab-paclitaxel, SGVSGHV-nab-paclitaxel, nab-paclitaxel, or no treatment. Mice were sacrificed and tumors excised at 72 hrs, fixed in 4% paraformaldehyde overnight and embedded in paraffin. Sections of 8 μm thickness were immunostained for cleaved caspase-3 using appropriate primary and secondary antibodies. Vasculature was immunostained using rabbit anti-von Willebrand factor antibody (Dako) and detected using DAB method. Paraffin sections were counterstained with hematoxylin. Light microscopy images captured on a Zeiss Axiophot widefield microscope at 10x.

Western Blotting

Tissue samples were homogenized, lysed in sample buffer, and membrane proteins extracted using a mammalian membrane protein extraction kit (Mem-PER Eukaryotic Membrane protein extraction kit, Pierce) prior to being coprecipitated with the HVGGSSV peptide-

biotin on streptavidin. Precipitated protein was then resolved on a 5-10% gradient SDS-polyacrylamide electrophoresis gel. The proteins were then transferred to a polyvinylidene difluoride membrane, blocked, and probed with an anti-TIP-1 antibody and appropriate secondary antibody.

Results

Radiation-targeted peptides

Phage displayed peptide libraries were used to identify amino acid sequences that bind specifically to irradiated cancers. The peptide ligand HVGGSSV bound within irradiated lung cancers. Co-precipitation of the HVGGSSV peptide revealed a putative receptor, taxinteracting protein-1 (TIP-1) that binds HVGGSSV. Membrane protein western blots showed a significant increase in the expression of TIP-1 protein at 4 and 24 hrs following irradiation with 3 Gy as compared to 0 Gy untreated control tumors (Figure 1A). Immunohistochemical staining showed significant levels of the TIP-1 membrane protein present in irradiated tumors, but not in untreated controls (Figure 1B). Near-infrared imaging studies showed significant targeting and binding of rabbit anti-TIP-1 IgG polyclonal antibody to irradiated tumors compared to untreated tumors and rabbit IgG controls at 72 hrs (Figure 1 C). Further studies performed using guinea pig and mouse anti-TIP-1 IgG antibodies validated binding within irradiated tumors (Figure 1C). Results from near-infrared imaging studies showed that the radiance from anti-TIP-1 antibodies was 1.93 ± 2.04 photons/s/cm^2/sr greater radiance compared to control IgG antibodies in irradiated tumors ($p \leq 0.08$) (Figure 1D).

The purpose of this study was to determine whether targeting nab-paclitaxel to radiation-inducible receptors improved tumor-specific drug delivery. To evaluate the tumor targeting ability of radiation-guided nab-paclitaxel, we studied *in vivo* near-infrared fluorescence imaging of the biodistribution in mice with heterotopic lung cancer tumors. We conjugated the HVGGSSV peptide to nab-paclitaxel via a bifunctional polyethylene glycol linker. The HVGGSSV peptide was then labeled with a fluorescent probe (Alexa fluor 750) for near-infrared fluorescence imaging studies. A scrambled sequence peptide (SGVSGHV) was used as a negative control. Nab-paclitaxel particles with no peptide conjugation were also fluorescently labeled and used as controls. Nude mice bearing subcutaneous Lewis lung carcinoma (LLC) tumors were treated with 3 Gy or 0 Gy radiation and administered HVGGSSV-nab-paclitaxel, SGVSGHV-nab-paclitaxel, or nab-paclitaxel. Images were acquired at 24, 48 and 72 hrs post-injection. Near-infrared images taken at 72 hrs after nab administration showed binding in irradiated tumors treated with HVGGSSV-nab-paclitaxel, whereas tumors treated with SGVSGHV-nab-paclitaxel or nab-paclitaxel alone showed minimal radiance (Figure 2A). Untreated (0 Gy) control tumors showed similar levels of radiance across all treatment groups (Figure 2A). Irradiated tumors treated with HVGGSSV-nab-paclitaxel showed 1.48 ± 1.66 photons/s/cm^2/sr greater radiance compared to SGVSGHVnab-paclitaxel, and 1.49 ± 1.36 photons/s/cm^2/sr greater than nab-paclitaxel alone ($p<0.05$) (Figure 2B). We found no significance difference in radiance from tumors treated with 2 Gy compared to 3 Gy during imaging of HVGGSSV-nab-paclitaxel (data not shown). To determine whether HVGGSSV binds to TIP-1 in tumor microvasculature, antibody blocking studies were performed. Near-infrared imaging showed that pre-blocking the TIP-1 receptor by administration of rabbit anti-TIP-1 IgG polyclonal antibody, followed by injection of HVGGSSV-nab-paclitaxel produced a marked decrease in radiance in irradiated tumors compared to control IgG antibody (Figure 2C). Blocking of TIP-1 resulted in a 47.6 fold drop in binding as compared to control IgG (Figure 2D).

Targeting nab-paclitaxel to irradiated cancer improves biodistribution

To determine whether HVGGSSV-nab-paclitaxel binds within tumor microvasculature, we labeled HVGGSSV-nab-paclitaxel, SGVSGHV-nab-paclitaxel and nab-paclitaxel with fluorescent probe Alexa fluor 594 prior to injection. Approximately 3 hrs after treatment, mice were sacrificed, and tumors were excised and cryopreserved for fluorescence microscopy. Tissue slices were fluorescently stained for von Willebrand factor (vWF), an endothelial cell marker. Figure 3 shows strong colocalization of targeted HVGGSSV-nab-paclitaxel with vascular endothelium in irradiated tumors (Figure 3A), but not in unirradiated tumors (Figure 3B) or TIP-1 blocked tumors. Scrambled SGVSGHV-nab-paclitaxel did not show significant colocalization in either irradiated or unirradiated tumors. Some colocalization was observed with nab-paclitaxel treatment in both irradiated and unirradiated groups. This suggests that HVGGSSV peptide enables binding of nab-paclitaxel within irradiated tumor microvasculature as early as 3 hrs after irradiation.

The ability of targeted HVGGSSV-nab-paclitaxel to localize and bind specifically to irradiated tumors was examined by biodistribution analysis in mice bearing LLC murine lung carcinoma. Paclitaxel levels were quantified in tumors, blood and organs 72 hrs following intravenous injection of either HVGGSSV-nab-paclitaxel, SGVSGHV-nab-paclitaxel or nab-paclitaxel. The results of this biodistribution analysis show that significantly higher levels of paclitaxel accumulated in irradiated tumors treated with HVGGSSV-nab-paclitaxel compared to SGVSGHV-nab-paclitaxel or nab-paclitaxel, and untreated control tumors (0 Gy) after 72 hrs. Figure 4A shows more than 5-fold increase in paclitaxel levels within irradiated tumors in HVGGSSV-nab-paclitaxel treated groups as compared to either nab-paclitaxel or SGVSGHV-nab-paclitaxel at 72 hrs. No significant difference in paclitaxel levels were observed in any unirradiated tumors. Biodistribution in organs showed similar paclitaxel levels distributed among heart, lungs, kidneys, liver and brain, with slightly less in the lungs and more in the brain. Figure 4B shows tumor to plasma ratios for HVGGSSV-nab-paclitaxel, SGVSGHV-nab-paclitaxel and nab-paclitaxel at 72 hours post-treatment. HVGGSSV nab-paclitaxel has a tumor/plasma ratio approximately 4-fold higher in irradiated tumors than unirradiated tumors, and 4-fold higher as compared to SGVSGHV-nab-paclitaxel. No significant difference was observed between irradiated and unirradiated SGVSGHV-nab-paclitaxel treated groups. A slight increase in tumor/plasma ratio was observed in nab-paclitaxel following tumor irradiation as compared to no irradiation. HVGGSSV-nab-paclitaxel had a tumor/plasma ratio approximately 3-fold higher than nab-paclitaxel in irradiated tumors.

Figure 4C shows immunohistochemical staining of paclitaxel in tumor tissues at 12 hrs post-treatment. Greater paclitaxel staining was observed in irradiated HVGGSSV-nab-paclitaxel treated tumors compared to unirradiated tumors, as well as SGVSGHV-nab-paclitaxel controls. Treatment with nab-paclitaxel resulted in similar paclitaxel staining between irradiated and unirradiated tumors. Irradiated tumors treated with HVGGSSV-nab-paclitaxel showed comparable levels of paclitaxel staining compared to nab-paclitaxel treated tumors. Targeting HVGGSSV-nab-paclitaxel to irradiated tumors increased the amount of paclitaxel delivered to tumors, and simultaneously decreased the amount of paclitaxel within other organs and tissues.

Targeted nab-paclitaxel enhances therapeutic efficacy

Therapeutic efficacy of HVGGSSV guided nab-paclitaxel was studied in two tumor models, murine Lewis lung carcinoma and NCI-H460 human large cell lung carcinoma grafted subcutaneously in C57 and athymic nude mice, respectively. On day 7 after tumor cell implantation, mice were injected with 10 mg/kg i.v. of either HVGGSSV-nab-paclitaxel, SGVSGHV-nab-paclitaxel, nab-paclitaxel, or saline. Tumor volumes for each treatment

group were measured manually with calipers until they reached a 4-fold increase in volume. Figure 5A and B show radiation alone (9 Gy) achieved only a slight tumor growth delay (2 days) in LLC tumors, and 6 days in H460 tumors as compared to untreated controls. Negative SGVSGHV-nab-paclitaxel controls showed no significant growth delay in LLC tumors and only 2 days delay in H460. After subsequent irradiation, this was improved to 2 days (LLC) and 6 days (H460). Treatment with nab-paclitaxel alone produced tumor growth delay of 2 days (LLC) and 6 days (H460), and upon additional irradiation increased to 6 days (LLC) and 11 days (H460). Both LLC and H460 lung carcinoma showed significant tumor growth delay for HVGGSSV-nab-paclitaxel as compared to nab-paclitaxel, SGVSGHV-nab-paclitaxel and saline controls (Figure 5A,B). HVGGSSV-nab-paclitaxel treatment achieved a growth delay of 3.4 days (LLC) and 8 days (H460). Additional irradiation increased this to 10 days (LLC) and 15 days (H460) over untreated controls. Subsequent doses of radiation improved growth delay for both HVGGSSV-nab-paclitaxel and nab-paclitaxel control. HVGGSSV-nab-paclitaxel combined with irradiation resulted in significantly greater tumor growth delay compared to tumors treated with SGVSGHV-nab-paclitaxel and irradiation or nab-paclitaxel and irradiation ($p<0.01$, Kruskal-Wallis).

To evaluate the mechanism of cell death, tumor sections were immunostained for caspase-3 expression, an apoptosis marker. As shown in Figure 5c, HVGGSSV-nab-paclitaxel treatment induced significant apoptosis in the irradiated tumors but not in the unirradiated tumors. Treatment with nab-paclitaxel alone produced greater apoptosis in irradiated tumors compared to unirradiated tumors. Results for HVGGSSV-nab-paclitaxel and nab-paclitaxel were similar for both irradiated groups, as compared to SGVSGHV-nab-paclitaxel and negative controls. Tumor sections were stained for the endothelial cell marker, von Willebrand factor (vWF) to evaluate tumor vascularity. As shown in Figure 5d, HVGGSSV-nab-paclitaxel treatment induced a significantly greater loss in vasculature in irradiated tumors compared to unirradiated tumors, nab-paclitaxel, SGVSGHV-nab-paclitaxel, and untreated controls. Treatment with nab-paclitaxel decreased vascular density compared with negative controls, but did not show a significant decrease between irradiated and unirradiated tumors. There was no difference in the vessel density between the groups treated with SGVSGHV-nab-paclitaxel and untreated controls.

Discussion

Cancer-selective therapy using various targeted strategies include antibodies, peptides, aptamers, and other targeting moieties that bind to receptors or antigens that are specific to cancer (1,3,6,7,36-39). Radiation can be used to induce the expression of receptors within tumor microvasculature (19-22). Tumor targeting peptides were developed to bind to these radiation-inducible receptors. These peptides can then be modified with nanoparticles containing cytotoxic drugs to create radiation-guided drug delivery systems. Previously, the GIRLRG peptide has been used to target the GRP78 receptors in breast and brain tumors, but not lung cancer models (21). In that study, the GRP78 ligand was conjugated to a non-GMP nanoparticle preparation, poly(valerolactoneepoxyvalerolactone-allylvalerolactone-oxepanedione) containing 11% epoxide and cross-linked with 1 equivalent of 2,2-(ethylenedioxy) bis (ethylamine) per epoxide. The current study focuses on the use of the HVGGSSV peptide for targeting the TIP-1 receptor expressed in non-small cell lung cancer models for cancer specific delivery of Abraxane (GMP-ready) (23). The advantage in the present approach is that it provides a means to target Abraxane specifically to irradiated lung cancer.

These peptide ligands can be used to functionalize nanoparticle carriers for radiation-guided delivery of chemotherapeutic drugs to tumor microvasculature (19-22,24). This strategy has the potential to increase the therapeutic ratio by delivering chemotherapy specifically to

tumors and reducing toxic side effects from non-specific delivery commonly produced by systemic chemotherapy. In this study, we found that the chemotherapeutic drug nab-paclitaxel can be targeted specifically to tumors using the radiation-guided peptide HVGGSSV. Furthermore, this modified nab-paclitaxel produced a significantly improved biodistribution profile and enhanced tumor bioavailability resulting in greater therapeutic efficacy in the treatment of cancer. The biodistribution of nab-paclitaxel was significantly improved when modified with HVGGSSV. This enhanced delivery of drug to the tumor site also translated to improved tumor growth delay compared to nab-paclitaxel. Accumulation of HVGGSSV-nab-paclitaxel within blood vessels of tumors was shown at 3 hrs and continued up to 72 hrs.

Concomitant administration of Paclitaxel enhances the efficacy of ionizing radiation and improves cure rates in lung cancer (30,31). In the present study, this enhanced radiation sensitivity combined with diminished vascular density in tumors improved tumor growth delay compared to nab-paclitaxel alone or in combination with radiation. The primary goal of this research was to demonstrate preclinical proof of concept. We studied 2 and 3 Gy, because we plan clinical trials in patients receiving 2 or 3 Gy. One and 5 Gy doses are clinically less meaningful doses. We found no difference in HVGGSSV binding in tumors treated with 2 compared to 3 Gy (data not shown). Further studies are necessary to determine whether this tumor-selective delivery can translate to reduced side effects and better treatment outcomes in lung cancer patients.

Acknowledgments

This work was supported by US National Cancer Institute grants R21-CA128456-02, 5R01-CA125757-03, 5R01-CA112385-05 and P50-CA128323 (D.E.H).

References

1. Arap W, Pasqualini R, Ruoslahti E. Cancer treatment by targeted drug delivery to tumor vasculature in a mouse model. Science. 1998; 279:377–380. [PubMed: 9430587]
2. Sengupta S, Eavarone D, Capila I, et al. Temporal targeting of tumour cells and neovasculature with a nanoscale delivery system. Nature Letters. 2005; 436:568–572.
3. Karmali PP, Kotamraju V, Kastantin M, et al. Targeting of albumin-embedded paclitaxel nanoparticles to tumors. Nanomedicine. 2009; 5:73–82. [PubMed: 18829396]
4. Desai N, Trieu V, Yao Z, et al. Increased antitumor activity, intratumor paclitaxel concentrations, and endothelial cell transport of cremophor-free, albumin-bound paclitaxel, ABI-007, compared with Cremophor-based paclitaxel. Clinical Cancer Research. 2006; 12:1317–1324. [PubMed: 16489089]
5. Allen TM, Cullis PR. Drug delivery systems: entering the mainstream. Science. 2004; 303:1818–1822. [PubMed: 15031496]
6. Peer D, Karp JM, Hong S, et al. Nanocarriers as an emerging platform for cancer therapy. Nature Nanotechnology. 2007; 2:751–760.
7. Davis ME, Chen Z, Shin DM. Nanoparticle therapeutics: an emerging treatment modality for cancer. Nature Reviews. 2008; 7:771–782.
8. Foote M. Using nanotechnology to improve the characteristics of antineoplastic drugs: improved characteristics of nab-paclitaxel compared with solvent-based paclitaxel. Biotechnology Annual Reviews. 2007; 13:345–357.
9. Hawkins MJ, Soon-shiong P, Desai N. Protein nanoparticles as drug carriers in clinical medicine. Advanced Drug Delivery Reviews. 2008; 60:876–885. [PubMed: 18423779]
10. Kratz F. Albumin as a drug carrier: design of prodrugs, drug conjugates and nanoparticles. Journal of Control Release. 200810.1016/j.jconrel.2008.05.010

11. Vogel SM, Minshall RD, Pilipovic M, Tiruppathi C, Malik AB. Albumin uptake and transcytosis in endothelial cells in vivo induced by albumin-binding protein. American journal of physiology. 2001; 281:L1512–L1522. [PubMed: 11704548]
12. Tiruppathi C, Song W, Bergenfeldt M, Sass P, Malik AB. Gp60 activation mediates albumin transcytosis in endothelial cells by tyrosine kinase-dependent pathway. The Journal of Biological Chemistry. 1997; 272:25968–25975. [PubMed: 9325331]
13. Minshall RD, Tiruppathi C, Vogel SM, et al. Endothelial cell-surface gp60 activates vesicle formation and trafficking via G(i)-coupled Src kinase signaling pathway. The Journal of Cell Biology. 2000; 150:1057–1070. [PubMed: 10973995]
14. John TA, Vogel SM, Tiruppathi C, Malik AB, Minshall RD. Quantitative analysis of albumin uptake and transport in the rat microvessel endothelial monolayer. American journal of physiology. 2003; 284:L187–L196. [PubMed: 12471015]
15. Damascelli B, Patelli GL, Lanocita R, et al. A novel intraarterial chemotherapy using paclitaxel in albumin nanoparticles to treat advanced squamous cell carcinoma of the tongue: preliminary findings. American Journal Roentgenology. 2003; 181:253–60.
16. Gradishar WJ, Tjulandin S, Davidson N, et al. Phase III trial of nanoparticle albumin-bound paclitaxel compared with polyethylated castor oil-based paclitaxel in women with breast cancer. Journal of Clinical Oncology. 2005; 23:7794–7803. [PubMed: 16172456]
17. Green MR, Manikhas GM, Orlov S, et al. Abraxane, a novel cremophor-free, albumin-bound particle form of paclitaxel for the treatment of advanced non-small-cell lung cancer. Annals of Oncology. 2006; 17:1263–1268. [PubMed: 16740598]
18. Lee T, Lin C, Kuo S, Chang D, Wu H. Peptide-mediated targeting to tumor blood vessels of lung cancer for drug delivery. Cancer Research. 2007; 67:10958–10965. [PubMed: 18006841]
19. Hallahan DE, Geng L, Qu S, et al. Integrin-mediated targeting of drug delivery to irradiated tumor blood vessels. Cancer Cell. 2003; 3:63–74. [PubMed: 12559176]
20. Hariri G, Zhang Y, Fu A, et al. Radiation-guided P-selectin antibody targeted to cancer. Annals of Biomedical Engineering. 2008; 36:821–830. [PubMed: 18273706]
21. Passarel1a RJ, Spratt DE, van der Ende AE, et al. Targeted nanopartic1es that deliver a sustained, specific release of Pac1itaxel to irradiated tumors. Cancer Res. 2010; 70:4550–9. [PubMed: 20484031]
22. Pattilo CB, Venegas B, Donelson FJ, et al. Radiation-guided targeting of combretastatin encapsulated immunoliposomes to mammary tumours. Pharm Res. 2009; 26:1093–100. [PubMed: 19172383]
23. Han Z, Fu A, Wang H, et al. Noninvasive assessment of cancer response to therapy. Nature Medicine. 2008; 14:343–349.
24. Pasqualini R, Ruoslahti E. Organ targeting in vivo using phage display peptide libraries. Nature. 1996; 380:364–366. [PubMed: 8598934]
25. Hallahan DE, Qu S, Geng L, et al. Radiation-mediated control of drug delivery. American Journal of Clinical Oncology. 2001; 24:473–480. [PubMed: 11586099]
26. Geng L, Osusky K, Konjeti S, Fu A, Hallahan DE. Radiation-guided drug delivery to tumor blood vessels results in improved tumor growth delay. Journal of Controlled Release. 2004; 99:369–381. [PubMed: 15451595]
27. Gardner ER, Dahut W, Figg WD. Quantitative determination of total and unbound paclitaxel in human plasma following Abraxane treatment. Journal of Chromatography B. 2008; 862:213–218.
28. Wiedenmann N, Valdecanas D, Hunter N, et al. 130-nm albumin-bound paclitaxel enhances tumor radiocurability and therapeutic gain. Clinical Cancer Research. 2007; 13:1868–1874. [PubMed: 17363543]
29. Hong JW, Lee IH, Kwak YH, et al. Efficacy and tissue distribution of DHP107, an oral paclitaxel formulation. Molecular Cancer Therapy. 2007; 6:3239–3247.
30. Dillman RO, Herndon J, Seagren SL, Eaton WL Jr, Green MR. Improved survival in stage III non-small cell lung cancer: seven year follow-up of cancer and leukemia group B (CALGB) 8433 trial. Journal of the National Cancer Institute. 1996; 88:1210–1215. [PubMed: 8780630]
31. Belani CP, Choy H, Bonomi P, et al. Combined chemoradiotherapy regimens of paclitaxel and carboplatin for locally advanced non-small cell lung cancer: a randomized phase II locally

advanced multi-modality protocol. Journal of Clinical Oncology. 2005; 23:5883–91. [PubMed: 16087941]

32. Curran WJ, Scott CB, Langer CJ, et al. Long-term benefit is observed in a phase III comparison of sequential vs. concurrent chemo-radiation for patients with unresected stage III non-small cell lung cancer. RTOG 9410. Proceedings of the American Society of Clinical Oncology. 2003; 22:621a.
33. Fournel P, Robinet G, Thomas P, et al. Randomized phase III trial of sequential chemoradiotherapy compared with concurrent chemoradiotherapy in locally advanced non-small cell lung cancer: Groupe Lyon-Saint-Etinne d'Oncologie Thoracique-Groupe Francais de Pneumo-Cancerologie NPC 95-01 Study. Journal of Clinical Oncology. 2005; 23:5910–5917. [PubMed: 16087956]
34. Furuse K, Fukuoka M, Kawahara M, et al. Phase III study of concurrent versus sequential thoracic radiotherapy in combination with mitomycin, vindesine, and cisplatin in unresectable stage III non-small cell lung cancer. Journal of Clinical Oncology. 1999; 17:2692–9. [PubMed: 10561343]
35. Kruskal WH, Wallis WA. Use of ranks in one-criteria variance analysis. Journal of the American Statistics Association. 1952; 47:583–621.
36. Wu AM, Senter PD. Arming antibodies: prospects and challenges for immunoconjugates. Nature Biotechnology. 2005; 23:1137–46.
37. Milenic DE, Brechbiel MW. Targeting of radio-isotopes for cancer therapy. Cancer Biology and Therapy. 2004; 3:361–70. [PubMed: 14976424]
38. Tai W, Mahato R, Cheng K. The role of HER2 in cancer therapy and targeted drug delivery. Journal of Control Release. 201010.1016/j.jconrel.2010.04.009
39. Sugahara KN, Teesalu T, Karmali PP, et al. Coadministration of a tumor-penetrating peptide enhances the efficacy of cancer drugs. Science. 2010; 328:1031–5. [PubMed: 20378772]

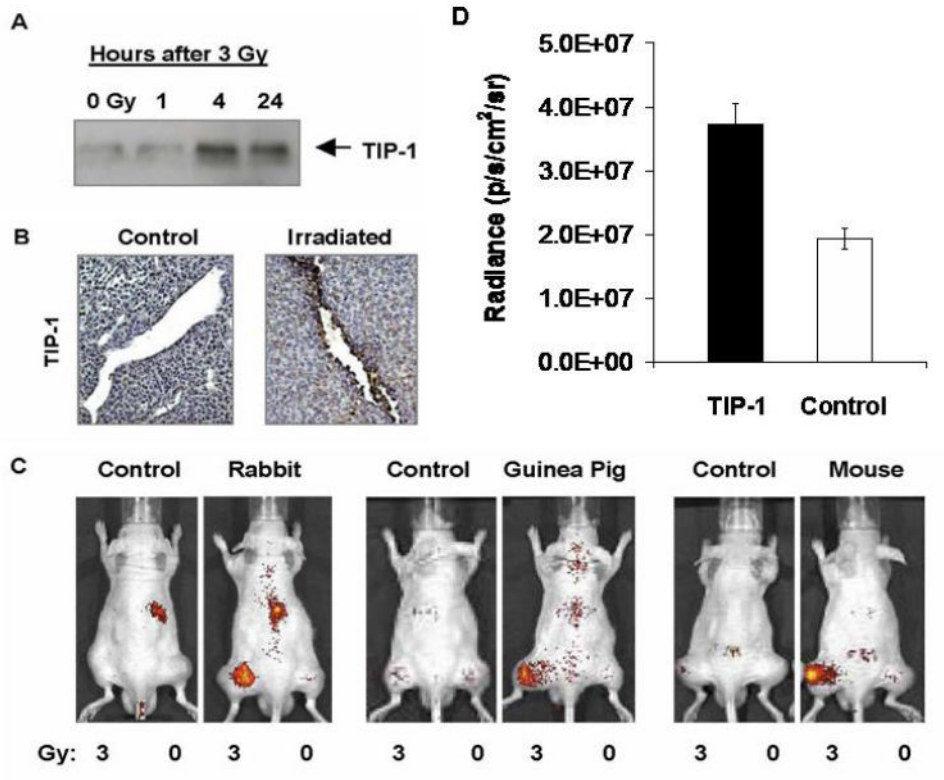

Figure 1. TIP-1 receptor targeting studies

a, Proteins were co-precipitated with the HVGGSSV peptide-biotin on streptavidin. Protein was separated by PAGE and transfers were incubated with polyclonal antibody to TIP-1. Shown is the autoradiograph of TIP-1 protein at 1, 4 and 24 hours after irradiation with 3 Gy compared to TIP-1 protein in untreated controls (0 Gy). **b**, Tumor sections were stained with anti-TIP-1 antibody. Shown are immunohistochemical sections of untreated control and irradiated tumor. **c**, LLC tumors grown in both hind limbs were treated with 3 Gy (left hind limb) or 0 Gy (right hind limb). Intravenous injection of Alexa fluor 750 labeled rabbit IgG antibody (control) and rabbit anti-TIP-1 polyclonal antibody; guinea pig IgG antibody (control) and guinea pig anti-TIP-1 polyclonal antibody; mouse IgG antibody (control) and mouse anti-TIP-1 monoclonal antibody. Shown are near-infrared (NIR) fluorescence images acquired approximately 72 hrs post-injection of mice. **d**. Bar graph of radiance for anti-TIP-1 antibodies vs. control IgG in irradiated tumors. Shown are the mean and SEM for 6-8 animals in each group. Unpaired Student's t test ($p \leq 0.08$).

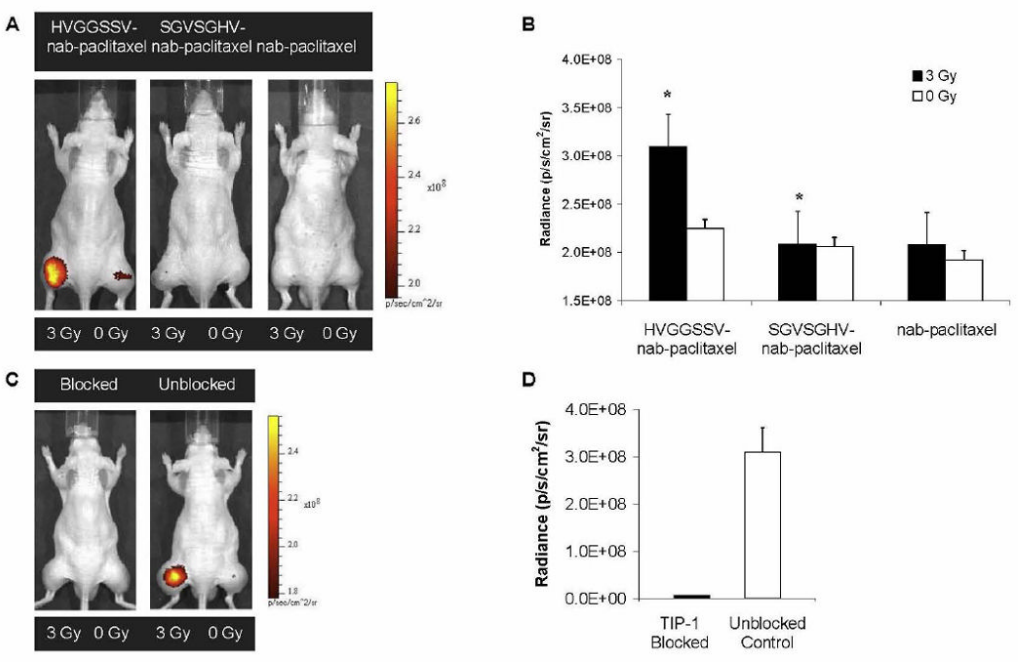

Figure 2. HVGGSSV-nab-paclitaxel targeted to irradiated tumors

a, LLC tumors grown in both hind limbs were treated with 3 Gy (left hind limb) or 0 Gy (right hind limb). Near-infrared (NIR) images acquired 72 hrs post-injection of mice after intravenous injection of Alexa fluor 750 labeled HVGGSSV-nab-paclitaxel, SGVSGHV-nab-paclitaxel, and unconjugated nab-paclitaxel. All images normalized to the same scale. Radiance was measured for both irradiated (3 Gy) and untreated (0 Gy) tumors. **b**, Bar graph of radiance for all treatment groups. The color scale bar indicates radiance in units of photons/s/cm^2/sr. Shown are the mean and SEM for five animals in each group. Unpaired Student's t test ($p<0.01$). **c**, To determine whether HVGGSSV specifically binds to TIP-1 in tumor microvasculature, TIP-1 blocking studies were also done using the same tumor model in nude mice and NIR imaging. Shown are NIR images of TIP-1 blocked and unblocked (control) mice. Tumors on the left hind limb were irradiated with 3 Gy and mice were given 50 μg of rabbit anti-TIP-1 polyclonal antibody intravenously 4 hrs later. Alexa fluor 750 labeled HVGGSSV-nab-paclitaxel was injected 2 hrs after antibody administration. Near-infrared imaging showed pre-blocking the TIP-1 receptor by administration of rabbit anti-TIP-1 IgG polyclonal antibody, followed by injection of HVGGSSV-nab-paclitaxel. **d**, Radiance was measured for both TIP-1 blocked and unblocked tumors as compared to pre-blocking with control IgG. Bar graph of radiance for both treatment groups, with mean and SEM for three animals in each group. Unpaired Student's t test ($p<0.01$).

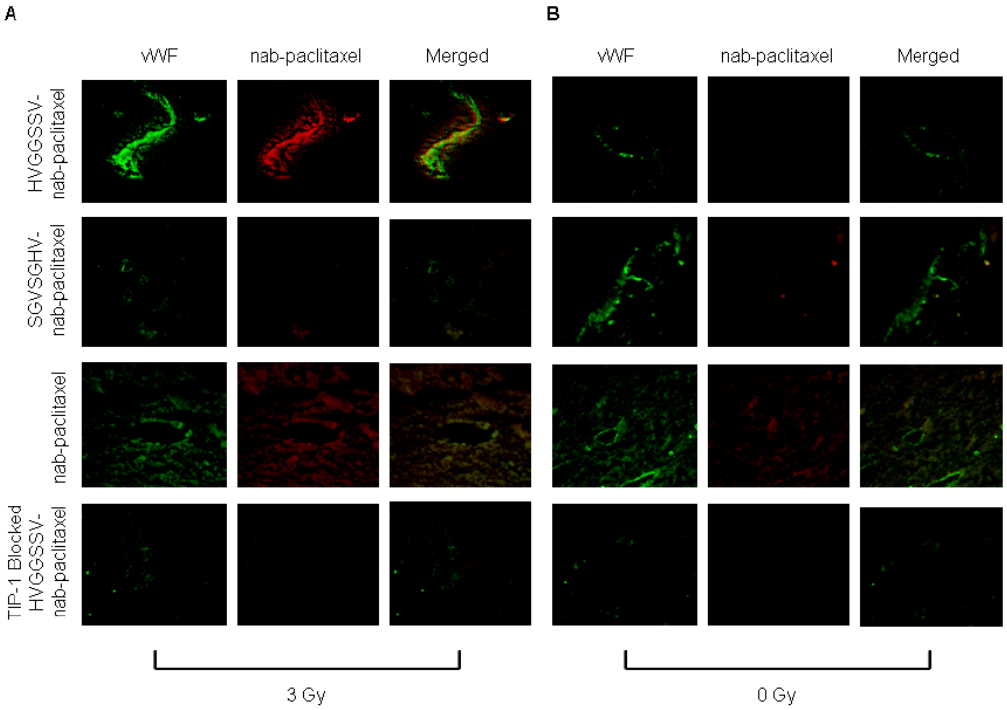

Figure 3. Colocalization HVGGSSV-nab-paclitaxel with tumor vascular endothelium

Cryosections of LLC tumors from each treatment group were stained for vascular marker von Willebrand factor (vWF) (green) 3 hrs after treatment with **a**, 3 Gy and **b**, 0 Gy. HVGGSSV-nab-paclitaxel, SGVSGHV-nab-paclitaxel, and nab-paclitaxel labled with Alexa fluor 594 (red) prior to injection.

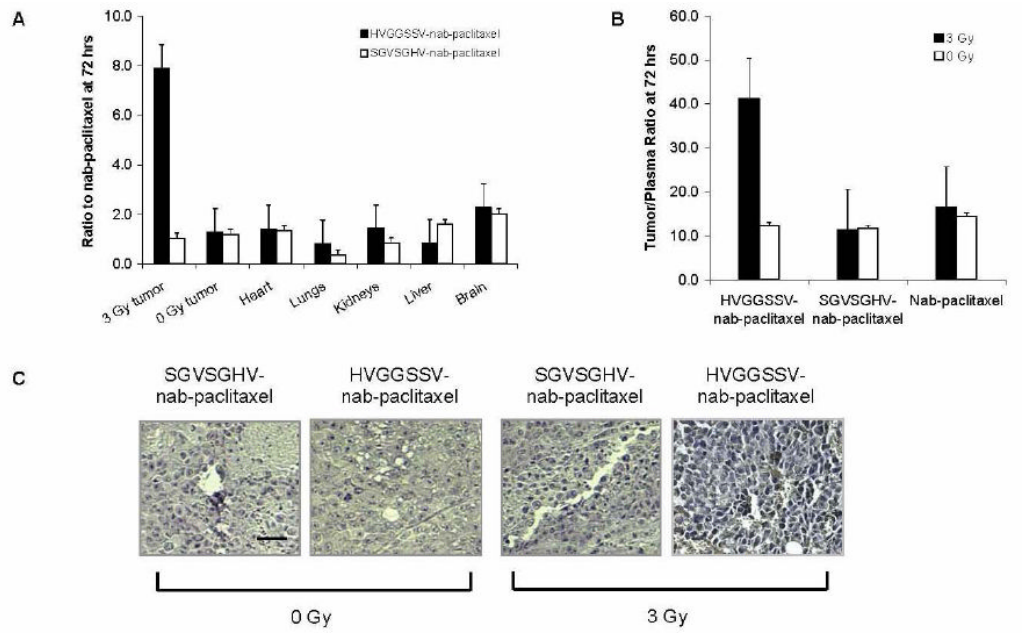

Figure 4. Biodistribution of targeted HVGGSSV-nab-paclitaxel

a, Biodistribution of paclitaxel in tumor and tissues in each treatment group compared to nab-paclitaxel. Shown are the mean and SEM from three animals in each group. **b**, Tumor/plasma concentration ratios at 72 hrs post-injection. Shown are the mean and SEM from three animals in each group. **c**, Shown are paraffin sections immunohistochemically stained for paclitaxel presence (brown), and counterstained with hematoxylin (blue). Nuclei stained brown were scored as positive and nuclei that stained blue were scored as negative. Scale bar, 50 μm.

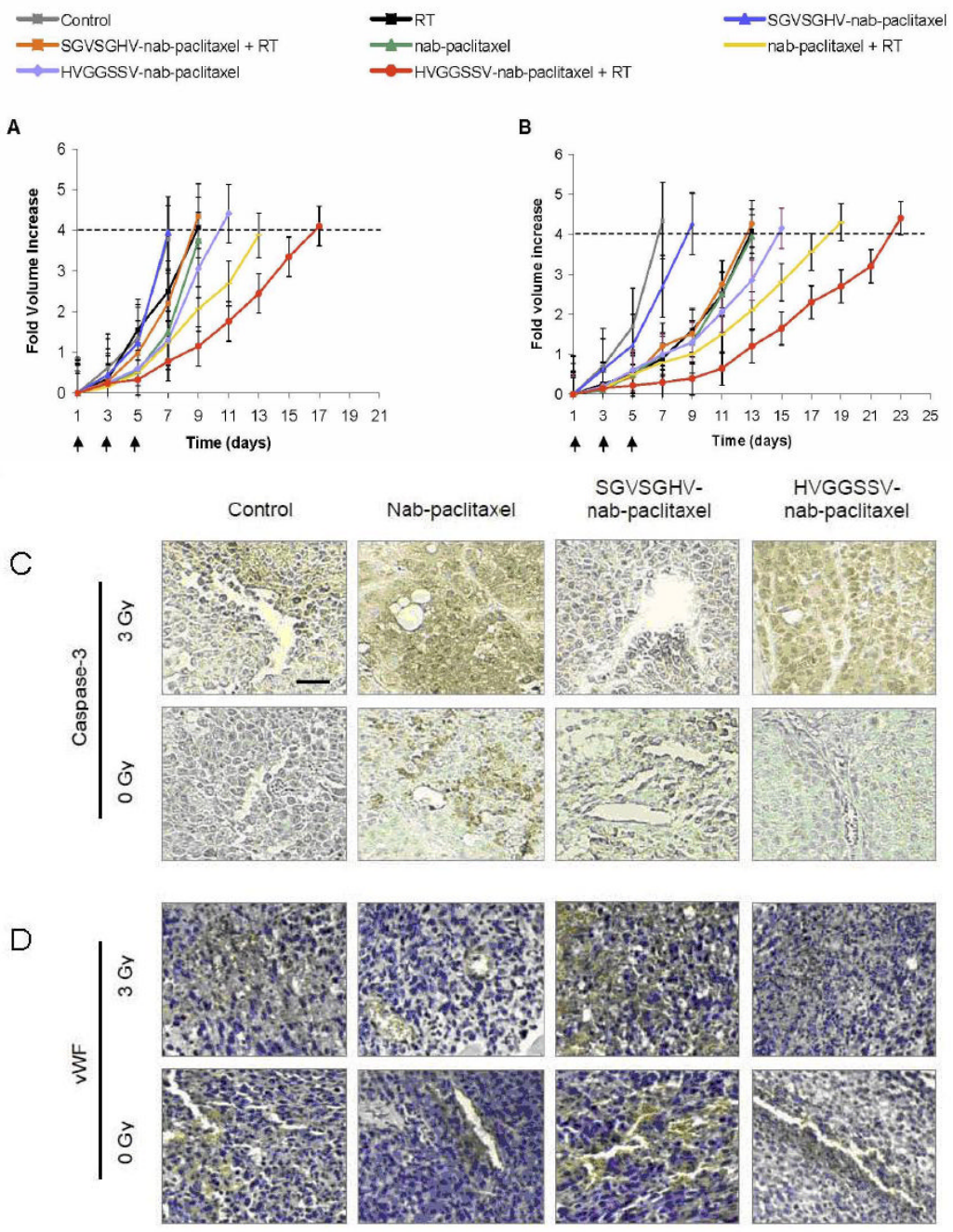

Figure 5. Therapeutic efficacy of targeted HVGGSSV-nab-paclitaxel in LLC and H460 xenografts

Tumor growth delay studies: **a**, LLC murine lung carcinoma bearing C57 mice or **b**, H460 bearing nude mice were treated with either 3 Gy or 0 Gy and injected i.v. 5 hrs later with either targeted HVGGSSV-nab-paclitaxel, nab-paclitaxel, SGVSGHV-nab-paclitaxel or saline. Arrows indicate daily irradiation with 3 Gy every other day. Shown are graphs of fold volume increase with mean and SEM from five animals in each group. HVGGSSV-nab-paclitaxel combined with irradiation resulted in significantly greater tumor growth delay compared to tumors treated with SGVSGHV-nab-paclitaxel and irradiation or nab-paclitaxel and irradiation ($p<0.01$, Kruskal-Wallis). Shown are immunohistochemical stains of LLC

tumor sections from each treatment group taken at 72 hrs after treatment initiation. **c**, Tissue slices were probed for active caspase-3 to identify cell death, and **d**, endothelial cell marker von Willebrand Factor (vWF) for vascular endothelium. All sections counterstained with hematoxylin. Brown stained nuclei were scored as positive and nuclei that stained blue were scored as negative. Paraffin sections, scale bar indicates 50 μm.